# Quasiparticles in the spin-fermion model for $CuO_2$ planes

Jan Bała
*Institute of Physics, Jagellonian University, Reymonta 4, PL-30059 Kraków, Poland*

Andrzej M. Oleś *
*Max-Planck-Institut für Festkörperforschung, Heisenbergstrasse 1, D-70569 Stuttgart, Federal Republic of Germany*

Jan Zaanen
*Lorentz Institute for Theoretical Physics, Leiden University, P.O.B. 9506, NL-2300 RA Leiden, The Netherlands*
(Received 12 April 1996)

The low-lying electron states in Mott-Hubbard insulators are quite well described using a self-consistent Born approximation in terms of spin-wave exchanges. This approach has been tested mainly in the context of the simplest ($t$-$J$) models. Here we present an extension to spin-fermion models, derived for realistic multiband models for the valence electrons in cuprate planes. The spectral functions show strong momentum dependences also at large energies, mimicking bandlike oxygen holes. In addition, a low-energy quasiparticle sector is found which can be interpreted in terms of propagating Zhang-Rice singlets. The quasiparticle dispersion is close to the one obtained with angular resolved photoemission in an insulating cuprate. [S0163-1829(96)03537-0]

## I. INTRODUCTION

The discovery of the high-$T_c$ superconductors[1] stimulated a large theoretical and experimental effort, but a full understanding of the electronic structure of high-temperature superconducting oxides (HTSO's) has not been reached so far. These compounds do not resemble the conventional superconductors and it is a generally accepted view that the detailed exploration of their normal-state properties is essential to the explanation of the high-temperature superconductivity. It is well known that band-structure calculations based on the local-spin-density approximation (LSDA) do not explain the large gaps observed in the angle-resolved (inverse) photoemission [AR(I)PES] experiments in transition-metal oxides (TMO's).[2] The large gaps in the $3d$ oxides as found by (inverse) photoemission experiments are at best underestimated by an order of magnitude, while in other cases LSDA even predicts metals.[3] Furthermore, the ground states of the parent compounds of HTSO's, $La_2CuO_4$, and $YBa_2Cu_3O_6$, are characterized by antiferromagnetic (AF) long-range order,[4] which is not reproduced by the band-structure calculations.[5] This demonstrates that electron correlations dominate in these systems.

The $t$-$J$ model has been derived from the multiband Hubbard model for HTSO's,[6–8] and one might believe that it provides the simplest approximation to the low-energy electronic states of strongly correlated TMO's and HTSO's. Compared to the ARPES experiments in HTSO's,[9,10] not enough intensity is found in the single-hole spectral function of the $t$-$J$ model at high energies. Instead, this spectral function is characterized by a single quasiparticle (QP) state at low energies, showing a small dispersion, while at higher energies one only finds a featureless incoherent background according to exact diagonalization studies.[11] Remarkably, this structure of the single-hole spectral function is accurately reproduced by an analytic approach[12,13] which starts from the powerful formalism of polaron theory,[14,15] and solves the problem in a self-consistent Born approximation (SCBA) introduced by Schmitt-Rink, Varma, and Ruckenstein.[14,15] Although originally devised as an asymptotic theory becoming correct only at low energies, it turns out to yield a quantitative description of the whole spectral function, including its behavior at large energies.

The $t$-$J$ model is only capable of describing the low-energy states. It is possible to catch a much larger fraction of the valence electrons without loosing the simplifications coming from spin-only physics: the spin-fermion models.[7,16] If the interest is in the oxygenlike valence band, the $3d$ degrees of freedom can be integrated out perturbatively as long as the upper (UHB) and lower (LHB) Hubbard bands are at high enough energy. What remains are O $2p$ holes, scattering against the $3d$ spin system. This condition is reasonably well satisfied in the cuprates, and this spin-fermion approach should therefore yield a realistic picture of the whole $2p$-like valence-band region. In the single-hole case, the collective excitations originate entirely in the spin system and the SCBA approach can be directly applied. This allows for a theoretical study of the whole valence band at binding energies less than $\simeq 8$ eV. We will show that in this AF background quantum effects dominate, determining the energy scale for the coherent QP motion. Such QP states are well known from the $t$-$J$ model,[2] where they were first recognized theoretically,[17] and then confirmed in exact diagonalization studies.[11,18–20] We show below that the QP states with small dispersions, found near the Fermi level, can be even quantitatively compared with recent photoemission results.[9,21] So far, these QP states have been studied in the charge-transfer (CT) model only in the $U\rightarrow\infty$ limit.[22]

We explored the SCBA before in the well documented context of NiO, where we obtained a quite appealing picture for the valence-band electronic structure.[23] Here we will focus on the perovskite planes of the cuprate superconductors.

 

Because the spin is smaller in the cuprates ($S=1/2$) than in the nickelates ($S=1$), the theory is, in principle, less well controlled but this does not seem to be an issue in light of the successes in the *t-J* context. In other regards, the cuprates are a better testing ground: (i) the planes are two dimensional and both the theory as the interpretation of the experiments become easier than for the three-dimensional NiO. (ii) Cuprates conform better to the charge-transfer limit than the nickelates, where the lower Hubbard band and the oxygen band nearly overlap. The spin-fermion model is therefore more realistic for the cuprate. (iii) The microscopy of the cuprates is better documented than that of the nickelates.

In Sec. II we will formulate a realistic multiband Hubbard model which takes into account all $3d$ and $2p$ states playing a role in planar directions. Assuming that the $d^{10}$ upper and $d^8$ lower band can be integrated out, we derive a spin-fermion model for the planar oxygen states, which includes the effects of the multiplet splittings of the LHB. Finally, the SCBA equations are derived for the self-energies and Green's functions, which are now in a matrix form because of the eight differently ''flavored'' oxygen states in the problem. A complete spin-fermion model contains two oxygen bands of $\sigma$ and two of $\pi$ symmetry which split in addition due to the scattering against the static Néel order.

In order to keep the numerical efforts on the tractable level, we have solved three simplified cases. First, we neglect the AF splitting of the oxygen orbitals in Sec. III, and consider there: (i) the two-band model which contains only O $p_\sigma$ orbitals, and (ii) a four-band model with O($2p_\sigma$) and O ($2p_\pi$) orbitals. Second, we treat in Sec. IV (iii) the two-band model of Sec. III including the AF splittings of the oxygen states. We will show that the quasiparticles with low dispersion are obtained in all cases, and will argue that the model which treats only the O $p_\sigma$ orbitals suffices to explain the QP states at low energy observed in the ARPES experiments of Wells *et al.* in the insulator $Sr_2CuO_2Cl_2$.[21]

## II. THE SPIN-FERMION MODEL

The simplest realistic model which describes the holes within the $CuO_2$ planes of HTSO's is the three-band model including Cu($3d_{x^2-y^2}$) and O($2p_\sigma$) orbitals.[24] Shortly after the discovery of the HTSO it was established that the system is strongly correlated,[25] and the electronic structure cannot be described in terms of conventional band-structure theory. These strong correlations result from the weak Cu-O hybridization as compared with the Coulomb repulsive energy at Cu sites, $U$, and the CT energy, $\Delta$. In this strong-coupling limit one can formulate effective Hamiltonians of the spin-fermion variety: at energies less than $U$ or $U-\Delta$, the $d$ electrons act as spins, and the oxygen holes interact with these Cu spins via Kondo interactions.[7,16] Neglecting interoxygen hoppings, one finds the oxygen states of local $b_1$ symmetry to couple strongly to the $3d_{x^2-y^2}$ orbitals, giving rise to the formation of Zhang-Rice singlets under doping,[6] while the states of $a_1$ symmetry do not hybridize with the holes on the Cu sites.

However, it is clear that a picture which results from the three-band model is seriously oversimplified. While it might give a qualitatively correct description of low-lying states, it cannot describe correctly the photoemission spectrum. The reason is that several $3d^8$ excited states are in the same energetic regime for realistic parameters of $CuO_2$ planes,[26–28] and only $^1E_1$ $3d^8$ state has been included in the three-band model.[29] This motivated us to derive a more complete and realistic spin-fermion model for the $CuO_2$ planes starting from a tight-binding model which includes all orbital degrees of freedom in the planar directions. This corresponds with seven orbitals per unit cell: three copper orbitals, $3d_{x^2-y^2}(d_x)$, $3d_{z^2-1}(d_z)$, and $3d_{xy}(d_{xy})$, and two orbitals at each oxygen ion, $2p_\sigma$ and $2p_\pi$. The holes interact by local Coulomb interactions at Cu sites.[24] In the strong-coupling limit we start from the localized ground state of the insulators, characterized by Cu $3d^9(x^2-y^2)$ and O $2p^6$ configurations, and described in terms of a $S=1/2$ Heisenberg quantum antiferromagnet.

After doping by one hole we consider the multiband charge-transfer model in the limit of weak hybridization. The ground-state manifold consists of the singly occupied copper ions and the doped holes within the oxygen orbitals. The transitions to the excited states, as caused by hybridization, lead to effective interactions between either a $2p_\sigma$ or a $2p_\pi$ doped hole, and the $3d_{x^2-y^2}$ holes of the AF background. We shall use the same generic picture as in the case of the three-band model, where these excited states belong to two Hubbard subbands: LHB and UHB.[30] The excited states which contribute to the LHB are (i) high-spin $^3A_2$ and $^3T_1$ triplets,

$$^3A_2(1)\sim d^\dagger_{iz\uparrow}d^\dagger_{ix\uparrow},\quad ^3A_2(0)\sim\frac{1}{\sqrt{2}}(d^\dagger_{iz\uparrow}d^\dagger_{ix\downarrow}+d^\dagger_{iz\downarrow}d^\dagger_{ix\uparrow}),$$

$$^3A_2(-1)\sim d^\dagger_{iz\downarrow}d^\dagger_{ix\downarrow}, \tag{2.1}$$

$$^3T_1(1)\sim d^\dagger_{ixy\uparrow}d^\dagger_{ix\uparrow},\quad ^3T_1(0)\sim\frac{1}{\sqrt{2}}(d^\dagger_{ixy\uparrow}d^\dagger_{ix\downarrow}+d^\dagger_{ixy\downarrow}d^\dagger_{ix\uparrow}),$$

$$^3T_1(-1)\sim d^\dagger_{ixy\downarrow}d^\dagger_{ix\downarrow}, \tag{2.2}$$

and (ii) three low-spin singlets, $^1A_2$, $^1E_1$, and $^1T_1$,

$$^1A_2(0)\sim\frac{1}{\sqrt{2}}(d^\dagger_{iz\uparrow}d^\dagger_{ix\downarrow}-d^\dagger_{iz\downarrow}d^\dagger_{ix\uparrow}),\quad ^1E_1(0)\sim d^\dagger_{ix\uparrow}d^\dagger_{ix\downarrow},$$

$$^1T_1(0)\sim\frac{1}{\sqrt{2}}(d^\dagger_{ixy\uparrow}d^\dagger_{ix\downarrow}-d^\dagger_{ixy\downarrow}d^\dagger_{ix\uparrow}), \tag{2.3}$$

where the fermion operators create holes in the different $d$ orbitals. This set of excited states can be divided into two groups: (i) $^3A_2$, $^1A_2$, and $^1E_1$ configurations with double occupied $e_g$-like $(x,z)$ orbitals; and (ii) $^3T_1$ and $^1T_1$ configurations with one hole in a $e_g$- and the second one in a $t_{2g}$-like $(xy)$ orbital. The UHB consists of the (local) CT excitations to the $2p^2_\sigma$ and $2p^1_\sigma 2p^1_\pi$ hole configurations accompanied by a transition to a $d^{10}$ configuration at the copper site.

Treating the virtual transitions to the high-energy states of the LHB and UHB perturbatively, one finds that the electronic states of the $CuO_2$ plane are described by the following spin-fermion model:

$$H=H_s+H^0_h+H^J_h+H_{h-s}. \tag{2.4}$$

It consists of the superexchange interaction between the Cu spins, $H_s$, the oxygen hole hopping terms, $H_h^0$ and $H_h^J$ and the Kondo interactions $H_{h-s}$ between the oxygen holes and copper spins. The latter are responsible for the quasiparticle behavior of the oxygen holes because they cause the dressing by the magnons of the AF lattice of copper spins.

The Kondo interactions are

$$H_{h-s}=\sum_{imn}\left[(J_{K,x^2-y^2}+J_{K,z^2})\mathbf{S}_i\cdot\mathbf{s}_{mn,\sigma}-J_{K,xy}\mathbf{S}_i\cdot\mathbf{s}_{mn,\pi}\right], \tag{2.5}$$

where $i$ are the copper sites, and $m$ and $n$ are the neighboring oxygen sites of the same Cu ion. $\mathbf{s}_{mn,\sigma(\pi)}$ are the (nonlocal) spin operators, which refer to $2p_\sigma$ and $2p_\pi$ orbitals,

$$s^+_{mn,\xi}=a^\dagger_{m,\xi\uparrow}a_{n,\xi\downarrow},$$

$$s^z_{mn,\xi}=\tfrac{1}{2}\left(a^\dagger_{m,\xi\uparrow}a_{n,\xi\uparrow}-a^\dagger_{m,\xi\downarrow}a_{n,\xi\downarrow}\right). \tag{2.6}$$

$a^\dagger_{m,\xi\uparrow(\downarrow)}$ are hole creation operators in a $\xi=\sigma,\pi$ orbital at site $m$. Notice that the $\sigma$ holes only communicate with the $e_g$-like $3d$ states, and the $\pi$ states only with the $xy$ $d$ orbital. The Kondo interactions in (2.5) are up to second order,

$$J_{K,x^2-y^2}=2[J_k(\Delta)+J_k(^1E_1)],$$

$$J_{K,z^2}=J_k(^1A_2)-J_k(^3A_2),\quad J_{K,xy}=J_k(^3T_1)-J_k(^1T_1), \tag{2.7}$$

with

$$J_k(\Delta)=\frac{t_x^2}{\Delta_\sigma},\quad J_k(^3A_2)=\frac{t_z^2}{U(^3A_2)-\Delta_\sigma+\Delta_{xz}},$$

$$J_k(^1A_2)=\frac{t_z^2}{U(^1A_2)-\Delta_\sigma+\Delta_{xz}},$$

$$J_k(^1E_1)=\frac{t_x^2}{U(^1E_1)-\Delta_\sigma},\quad J_k(^3T_1)=\frac{t_{xy}^2}{U(^3T_1)-\Delta_\pi},$$

$$J_k(^1T_1)=\frac{t_{xy}^2}{U(^1T_1)-\Delta_\pi}. \tag{2.8}$$

The first Kondo interaction is due to fluctuations to the UHB and the other five interactions involve the LHB. Here $\Delta_\sigma$ and $\Delta_\pi$ are the CT gaps between the hole energies on $p_\sigma$ and $p_\pi$ orbitals and the $d_{x^2-y^2}$ orbital, and $\Delta_{xz}$ is the crystal-field splitting between the $d_{3x^2-y^2}$ and $d_{z^2}$ orbitals. Notice the *ferromagnetic* sign of the Kondo interactions involving the high spin $d^8$ states.

The AF interactions between the $S=\frac{1}{2}$ spins on the Cu sites, $\mathbf{S}_i$, are given by the superexchange Hamiltonian

$$H_s=J\sum_{\langle ij\rangle\in(A,B)}\mathbf{S}_i\cdot\mathbf{S}_j, \tag{2.9}$$

where $A$ and $B$ are the sublattices of $\downarrow$ and $\uparrow$ spins in the Néel state, respectively, and the AF superexchange $J>0$ acts between nearest-neighbor Cu ions in the $CuO_2$ planes. The spin Hamiltonian $H_s$ may be expressed in terms of Schwinger bosons $b_{i\sigma}$.[15] The spin waves, as well as the hole-spin wave coupling are easily obtained by expanding around the Néel saddle point. To zeroth order, each site is occupied by a single Schwinger boson, and

$$b_{i\uparrow}=b_{j\downarrow}=0,\quad b_{i\downarrow}=b_{j\uparrow}=1, \tag{2.10}$$

where $i\in A$ and $j\in B$. Expanding to Gaussian order, one finds one branch of acoustic magnons with an energy $\omega_{\mathbf{q}}$.[15]

The kinetic energy in the oxygen bands is given by the direct oxygen-oxygen hopping, and by the effective second-order processes similar to those included in the Kondo hole-spin interactions, $H_{h-s}$. The direct oxygen-oxygen hybridization is of the form

$$H_h^0=\sum_{mns}\left[t_{mn}^{\sigma\sigma}a^\dagger_{m,\sigma s}a_{n,\sigma s}+t_{mn}^{\pi\pi}a^\dagger_{m,\pi s}a_{n,\pi s}+t_{mn}^{\sigma\pi}a^\dagger_{m,\sigma s}a_{n,\pi s}+\text{H.c.}\right], \tag{2.11}$$

with $t_{mn}^{\sigma\sigma}$, $t_{mn}^{\pi\pi}$ and $t_{mn}^{\sigma\pi}$ standing for $2p_\sigma-2p_\sigma$, $2p_\pi-2p_\pi$, and $2p_\sigma-2p_\pi$ interoxygen hoppings, respectively, and $s=\uparrow,\downarrow$. The sites $m$ and $n$ label the nearest-neighbor oxygen sites, and the hopping elements $t_{mn}^{\sigma(\pi)\sigma(\pi)}$ contain the phases of the respective orbitals.

In addition to the spin-fermion Kondo interaction Eq. (2.5), one finds as well the effective three-site hopping of the oxygen holes,

$$H_h^J=\sum_{imns}\left[(T_{x^2-y^2}+T_{z^2})a^\dagger_{m,\sigma s}a_{n,\sigma s}+T_{xy}a^\dagger_{m,\pi s}a_{n,\pi s}\right], \tag{2.12}$$

with the effective hopping terms determined by a two-step hopping via the Cu sites

$$T_{x^2-y^2}=\tfrac{1}{2}\left[J_k(\Delta)-J_k(^1E_1)\right],$$

$$T_{z^2}=-\tfrac{1}{4}\left[3J_k(^3A_2)+J_k(^1A_2)\right], \tag{2.13}$$

via $3d_{x^2-y^2}$ and $3d_{z^2}$ orbitals, and

$$T_{xy}=-\tfrac{1}{4}\left[3J_k(^3T_1)+J_k(^1T_1)\right], \tag{2.14}$$

via $3d_{xy}$ states. The sites $m$ and $n$ in Eq. (2.12) are the nearest-neighbor oxygen sites of the same Cu ion, and for this reason the three-site hopping couples as well the two oxygen orbitals along the $x$ ($y$) direction, unlike $H_h^0$

In the Néel state, as defined by Eq. (2.10), the Ising part of the Kondo interaction reduces to additional hoppings, which represent the scattering of the holes against the static Néel order parameter. These terms will cause AF splittings of the oxygen bands. Because the oxygen states living on the $A$ and $B$ sublattices become inequivalent, the number of oxygen bands doubles to eight and the calculations become much more tedious. Although these splittings are certainly not unimportant, they are not expected to change the picture completely and we will proceed with neglecting these splittings in first instance. It will be found that the states of $\pi$ and $\sigma$ symmetry are relatively weakly coupled and in Sec. IV we will consider the important $\sigma$ sector, including the effects of the hole scattering against the static order.

The hopping part of the effective Hamiltonian, $H_h^0+H_h^J$, can be easily diagonalized in the reciprocal space by introducing new oxygen operators $p_{\mathbf{k}\mu,\sigma}$, defined by the Fourier transformation

$$p_{\mathbf{k}\mu,s}=\frac{1}{\sqrt{N}}\sum_i a_{i\mu,s}e^{i\mathbf{k}\mathbf{r}_i}, \tag{2.15}$$

where the index $\mu=1,\ldots,4$ describes four different oxygen states in the unit cell: $p_{1\sigma}$, $p_{2\sigma}$, $p_{1\pi}$, and $p_{2\pi}$, respectively. With the help of these operators we write the explicit form of the hole hopping part of the Hamiltonian Eq. (2.4) as follows:

$$H_h^0+H_h^J=\sum_{\mathbf{k}\mu\mu' s}([H_h^0]_{\mu\mu'}+[H_h^J]_{\mu\mu'})p^\dagger_{\mathbf{k}\mu,s}p_{\mathbf{k}\mu',s}, \tag{2.16}$$

where, $H_h^0$ is the free hole hopping,

$$[H_h^0]=\begin{bmatrix}\varepsilon_\sigma & T_{pp} & 0 & T'_{pp}\\ T_{pp} & \varepsilon_\sigma & T'_{pp} & 0\\ 0 & T'_{pp} & \varepsilon_\pi & T_{pp}\\ T'_{pp} & 0 & T_{pp} & \varepsilon_\pi\end{bmatrix}, \tag{2.17}$$

with

$$T_{pp}=4t_{pp}\sin k_x\sin k_y,$$

$$T'_{pp}=-4t'_{pp}\cos k_x\cos k_y, \tag{2.18}$$

and the Cu-O distance (half of the unit cell length) $a=1$. $t_{pp}$ and $t'_{pp}$ are direct oxygen hoppings between the pairs of $2p_{\sigma(\pi)}$ and $2p_{\sigma(\pi)}$ orbitals, respectively. When we neglect the smaller hopping element (by taking $t'_{pp}=0$), which mixes the $2p_\sigma$ and $2p_\pi$ states, we find the two subbands for $p_\sigma$ and $p_\pi$ orbitals, respectively,

$$\varepsilon_{\sigma(\pi)}(\mathbf{k})=\varepsilon_{\sigma(\pi)}\pm 4t_{pp}\sin k_x\sin k_y. \tag{2.19}$$

Because the $\pi$ and $\sigma$ orbitals become independent in this case, $[H_h^J]$ is given by a block diagonal form which we write as a simple product $[H_h^J]=[H_h^J]_e\oplus[H_h^J]_t$, where the relevant parts of the $4\times4$ matrices are of the form,

$$[H_h^J]_\sigma=\begin{bmatrix}4(T_{x^2-y^2}+T_{z^2})\sin^2k_x & -4(T_{x^2-y^2}-T_{z^2})\sin k_x\sin k_y\\ -4(T_{x^2-y^2}-T_{z^2})\sin k_x\sin k_y & 4(T_{x^2-y^2}+T_{z^2})\sin^2k_y\end{bmatrix}, \tag{2.20}$$

and,

$$[H_h^J]_\pi=\begin{bmatrix}4T_{xy}\sin^2k_x & -4T_{xy}\sin k_x\sin k_y\\ -4T_{xy}\sin k_x\sin k_y & 4T_{xy}\sin^2k_y\end{bmatrix}. \tag{2.21}$$

Thus, we find that the mixing between $\sigma$ and $\pi$ states within $CuO_2$ planes is only due to $t'_{pp}$ hoppings, quite different from the similar spin-fermion model for NiO, where the three-site terms also contribute to the hopping between the oxygen orbitals of different symmetry.[23]

In the linear spin-wave (LSW) approximation one finds the magnon dispersion to be given by the standard expression for a two-dimensional (2D) Heisenberg antiferromagnet,

$$\omega_{\mathbf{q}}=2J(1-\gamma_{\mathbf{q}}^2)^{1/2}. \tag{2.22}$$

Performing Fourier,

$$b_{\mathbf{q}}=\frac{1}{\sqrt{N}}\sum_{i\in A}b_{i\uparrow}e^{i\mathbf{q}\cdot\mathbf{r}_i}+\frac{1}{\sqrt{N}}\sum_{j\in B}b_{j\downarrow}e^{i\mathbf{q}\cdot\mathbf{r}_j}, \tag{2.23}$$

and Bogoliubov transformations,

$$\beta_{\mathbf{q}}=u_{\mathbf{q}}b_{\mathbf{q}}-v_{\mathbf{q}}b^\dagger_{-\mathbf{q}},\quad u_{\mathbf{q}}=\left[\frac{1+(1-\gamma_{\mathbf{q}}^2)^{1/2}}{2(1-\gamma_{\mathbf{q}}^2)^{1/2}}\right]^{1/2},$$

$$v_{\mathbf{q}}=-\mathrm{sgn}(\gamma_{\mathbf{q}})\left[\frac{1-(1-\gamma_{\mathbf{q}}^2)^{1/2}}{2(1-\gamma_{\mathbf{q}}^2)^{1/2}}\right]^{1/2}, \tag{2.24}$$

with $\gamma_{\mathbf{q}}=1/z\Sigma_{\boldsymbol{\delta}}e^{i\mathbf{q}\boldsymbol{\delta}}$ (with $z=4$ in the 2D case), and neglecting an irrelevant constant one finds after somewhat lengthy but straightforward calculations the following Hamiltonian in LSW order:

$$H_{\mathrm{LSW}}=\sum_{\mathbf{k}\mu,s}\varepsilon_\mu(\mathbf{k})a^\dagger_{\mathbf{k}\mu,s}a_{\mathbf{k}\mu,s}+\sum_{\mathbf{q}}\omega_{\mathbf{q}}\beta^\dagger_{\mathbf{q}}\beta_{\mathbf{q}}$$
$$+\frac{1}{\sqrt{N}}\sum_{\mathbf{kq},\mu\nu s}M_{\mu\nu}(\mathbf{k},\mathbf{q})a^\dagger_{\mathbf{k}-\mathbf{q}\mu,s}a_{\mathbf{k}\nu,-s}(\beta^\dagger_{\mathbf{q}}+\beta_{-\mathbf{q}}), \tag{2.25}$$

with $s=1$ $(-1)$ for the spin $\uparrow$ $(\downarrow)$, respectively. $\varepsilon_\mu(\mathbf{k})$ with $\mu=1,\ldots,4$, stands for the four oxygen subbands

$$a_{\mathbf{k}\mu,s}=\sum_\xi V^\xi_{\mu,\mathbf{k}}p_{\mathbf{k}\xi,s}, \tag{2.26}$$

obtained before from the diagonalization (with the help of a matrix $V^\xi_{\mu,\mathbf{k}}$) of interoxygen hopping terms, $H_h^0+H_h^J$. Unlike in the $t$-$J$ model,[15] the spinless fermion describing the charge of the Cu holes is absent in the final Hamiltonian Equation (2.25) because the transition-metal spins are localized and the oxygen holes can be described as normal fermions, interacting with the magnons. The hole-magnon bare vertex

found in the LSW-SCBA, $M_{\mu\nu}(\mathbf{k},\mathbf{q})$, depends on the coefficients of the Bogoliubov transformations for fermions, $\{V^{\xi}_{\mu,\mathbf{k}}\}$, and for bosons, $\{u_{\mathbf{q}},\ v_{\mathbf{q}}\}$,

$$M_{\mu\nu}(\mathbf{k},\mathbf{q})=(u_{\mathbf{q}}+v_{\mathbf{q}})\sum_{\xi\eta} W^{\xi\eta}_{\mu\nu}(\mathbf{k},\mathbf{q})F_{\xi\eta}(\mathbf{k},\mathbf{q}), \quad (2.27)$$

with $W^{\xi\eta}_{\mu\nu}(\mathbf{k},\mathbf{q})=V^{\xi}_{\mu,\mathbf{k}}V^{\eta}_{\nu,\mathbf{k}-\mathbf{q}}$.

The functions $F_{\xi\eta}(\mathbf{k},\mathbf{q})$, determining the vertex $M_{\mu\nu}(\mathbf{k},\mathbf{q})$, are obtained by evaluating the second-order terms which originate in the hybridization between the $2p_{\sigma(\pi)}$ and $3d$ states of $e_g$ ($d_{x^2-y^2}$, $d_{3z^2-1}$) and $t_{2g}$ ($d_{xy}$) symmetry, respectively. Similarly to $[H^J_h]$, the functions $F_{\xi\eta}(\mathbf{k},\mathbf{q})$ have independent parts for $\sigma$ and $\pi$ orbitals with the following nonzero elements:

$$\begin{aligned}
F_{11}(\mathbf{k},\mathbf{q})&=(J_{k,x^2-y^2}+J_{k,z^2})[\cos q_x-\cos(2k_x-q_x)],\\
F_{12}(\mathbf{k},\mathbf{q})&=-2(J_{k,x^2-y^2}-J_{k,z^2})\sin k_x\sin(k_y-q_y),\\
F_{33}(\mathbf{k},\mathbf{q})&=J_{k,xy}[\cos q_x-\cos(2k_x-q_x)],\\
F_{34}(\mathbf{k},\mathbf{q})&=-2J_{k,xy}\sin k_x\sin(k_y-q_y).
\end{aligned} \quad (2.28)$$

$F_{22}(\mathbf{k},\mathbf{q})$, $F_{21}(\mathbf{k},\mathbf{q})$, $F_{44}(\mathbf{k},\mathbf{q})$, and $F_{43}(\mathbf{k},\mathbf{q})$ are obtained from $F_{11}(\mathbf{k},\mathbf{q})$, $F_{12}(\mathbf{k},\mathbf{q})$, $F_{33}(\mathbf{k},\mathbf{q})$, and $F_{34}(\mathbf{k},\mathbf{q})$, respectively, using the symmetry $(x,y)\Leftrightarrow(y,x)$.

As in the case of NiO,[23] we have determined the hole self-energy self-consistently in SCBA by iterating the Green functions

$$G^{-1}_{\mu\nu}(\mathbf{k},\omega)=\omega-\delta_{\mu\nu}\varepsilon_{\mu}(\mathbf{k})-\Sigma_{\mu\nu}(\mathbf{k},\omega) \quad (2.29)$$

with the hole self-energy obtained from the bare vertex and the self-consistently dressed Green function

$$\Sigma_{\mu\nu}(\mathbf{k},\omega)=\sum_{\alpha\beta,\mathbf{q}} M_{\mu\alpha}(\mathbf{k},\mathbf{q})M_{\beta\nu}(\mathbf{k},\mathbf{q})G_{\alpha\beta}(\mathbf{k}-\mathbf{q},\omega-\omega_{\mathbf{q}}). \quad (2.30)$$

This approximation has been shown to be surprisingly accurate for the $t$-$J$ model,[12] and has been used by us as well for systems with larger spins, $S=1$ (Ref. 23) and $S=3/2$.[31]

All the calculations were performed on a $16\times16$ lattice with torroidal boundary conditions. We present below the single-hole spectral functions ($\mu=1,\ldots,4$), obtained from such a procedure:

$$A_{\mu\mu}(\mathbf{k},\omega)=\frac{1}{\pi}\mathrm{Im}G_{\mu\mu}(\mathbf{k},\omega), \quad (2.31)$$

neglecting $\Sigma_{\mu\nu}(\mathbf{k},\omega)$ and $G_{\mu\nu}(\mathbf{k},\omega)$ for $\mu\neq\nu$ as they contribute only to higher-order diagrams.

The spin-fermion model Eq. (2.25) contains four oxygen bands, and will be called below a four-band model. To avoid some of the numerical complexity of SCBA, we have studied as well a simplified model which includes only the oxygen $p_{\sigma}$ orbitals. In this case one finds only the spectral functions $A_{\mu\mu}(\mathbf{k},\omega)$ of $e_g$-like symmetry. Although $x^2-y^2$ and $3z^2-1$ are coupled by the vertex function $M_{\mu\nu}(\mathbf{k},\mathbf{q})$, the resulting spectral functions have mostly either $d_{x^2-y^2}$ or $d_{z^2}$ character. Thus, we will use these labels below in discussing the numerical results. Finally, we will consider this ''$\sigma$ only'' model including the antiferromagnetic splittings in Sec. IV.

Knowing the Green function, it is instructive to obtain the wave function which in our model has the following form:[32,33]

$$\begin{aligned}
|\Psi^{(n)}_{\mathbf{k},i}\rangle=\sqrt{W^{\mathrm{QP}}_{\mathbf{k},i}}\Bigg[&a^{\dagger}_{\mathbf{k},i,\sigma}+N^{-1/2}\sum_{\mathbf{q}_1,i_1}M_{ii_1}(\mathbf{k},\mathbf{q}_1)G_{i_1}(\mathbf{k}_1,\omega_1)a^{\dagger}_{\mathbf{k}_1,i_1,-\sigma}\beta^{\dagger}_{\mathbf{q}_1}+\ldots\\
&+N^{-n/2}\sum_{\mathbf{q}_1\ldots\mathbf{q}_n,i_1\ldots i_n}M_{ii_1}(\mathbf{k},\mathbf{q}_1)G_{i_1}(\mathbf{k}_1,\omega_1)\ldots M_{i_{n-1}i_n}(\mathbf{k}_{n-1},\mathbf{q}_n)G_{i_n}(\mathbf{k}_n,\omega_n)a^{\dagger}_{\mathbf{k}_n,i_n,(-1)^n\sigma}\beta^{\dagger}_{\mathbf{q}_1}\ldots\beta^{\dagger}_{\mathbf{q}_n}\Bigg]|0\rangle,
\end{aligned} \quad (2.32)$$

with the momentum, $\mathbf{k}_i=\mathbf{k}-\mathbf{q}_1-\ldots-\mathbf{q}_i$, and energy $\omega_i=\varepsilon_{\mathbf{k}}-\omega_{\mathbf{q}_1}-\ldots-\omega_{\mathbf{q}_i}$ conservation satisfied by each term. $\varepsilon_i(\mathbf{k})=\Sigma_i(\mathbf{k},\varepsilon_i(\mathbf{k}))$ is the QP energy, and $W^{\mathrm{QP}}_{\mathbf{k},i}$ is the QP spectral weight given by

$$W^{\mathrm{QP}}_{\mathbf{k},i}=\frac{1}{1-(\partial/\partial\omega)\Sigma_i(\mathbf{k},\omega)\big|_{\omega=\varepsilon_i(\mathbf{k})}}. \quad (2.33)$$

In the present model there are several oxygen bands and this leads to a more complex form of the norm $N^{(n)}_{\mathbf{k}i}=\langle\Psi^{(n)}_{\mathbf{k}i}|\Psi^{(n)}_{\mathbf{k}i}\rangle$ than that known from the $t$-$J$ model,[33]

$$\begin{aligned}
\langle\Psi^{(n)}_{\mathbf{k},i}|\Psi^{(n)}_{\mathbf{k},i}\rangle=W^{\mathrm{QP}}_{\mathbf{k},i}\Bigg[&1+N^{-1}\sum_{\mathbf{q}_1,j}M^2_{ij}(\mathbf{k},\mathbf{q}_1)|G_j(\mathbf{k}_1,\omega_1)|^2+N^{-2}\sum_{q_1,q_2,j,i_1,i'_1}M_{ii_1}(\mathbf{k},\mathbf{q}_1)M_{i'_1i}(\mathbf{k},\mathbf{q}_1)\\
&\times G_{i_1}(\mathbf{k}_1,\omega_1)G^{*}_{i'_1}(\mathbf{k}_1,\omega_1)M_{i_1j}(\mathbf{k}_1,\mathbf{q}_2)M_{ji'_1}(\mathbf{k}_1,\mathbf{q}_2)|G_j(\mathbf{k}_2,\omega_2)|^2+\ldots\\
&+N^{-n}\sum_{q_1\ldots q_n,j,i_1\ldots i_{n-1},i'_1\ldots i'_{n-1}}M_{ii_1}(\mathbf{k},\mathbf{q}_1)M_{i'_1i}(\mathbf{k},\mathbf{q}_1)G_{i_1}(\mathbf{k}_1,\omega_1)
\end{aligned}$$

$$\times G^{*}_{i'_1}(\mathbf{k}_1,\omega_1)M_{i_1 i_2}(\mathbf{k}_1,\mathbf{q}_2)M_{i'_2 i'_1}(\mathbf{k}_1,\mathbf{q}_2)G_{i_2}(\mathbf{k}_2,\omega_2)G^{*}_{i'_2}(\mathbf{k}_2,\omega_2)\times\ldots$$

$$\times M_{i_{n-2} i_{n-1}}(\mathbf{k}_{n-2},\mathbf{q}_{n-1})M_{i'_{n-1} i'_{n-2}}(\mathbf{k}_{n-2},\mathbf{q}_{n-1})G_{i_{n-1}}(\mathbf{k}_{n-1},\omega_{n-1})$$

$$\times G^{*}_{i'_{n-1}}(\mathbf{k}_{n-1},\omega_{n-1})M_{i_{n-1} j}(\mathbf{k}_{n-1},\mathbf{q}_n)M_{j i'_{n-1}}(\mathbf{k}_{n-1},\mathbf{q_n})|G_j(\mathbf{k}_n,\omega_n)|^2\Big]|0\rangle. \quad (2.34)$$

## III. NUMERICAL RESULTS FOR THE TWO-BAND AND FOUR-BAND SPIN-FERMION MODEL

Before studying the complete hole-magnon Hamiltonian Eq. (2.25) derived in Sec. II, we shall present the results obtained with the simplified spin-fermion model, which is derived from the four-band model[34] for the $CuO_2$ plane, and deals only with the two $\sigma$-type oxygen hole bands, dressed by hole-magnon couplings of $e_g$ symmetry. Such a two-band spin-fermion model is expected to reproduce already some essential features seen in photoemission, because the coupling with the $\pi$ sector is relatively weak, and has the advantage of being more transparent than the full model Eq. (2.25) which involves the $\pi$ states as well.

Realistic parameters for $CuO_2$ planes have been obtained by several authors.[26–28] These have been either extracted from the LDA band-structure calculations mapped on the energy surface of the tight-binding model with local electron-electron interactions,[26,27,35–37] or deduced from photoemission experiments.[28,38,39] Here we use the multiplet structure of the $3d^8$ configuration and the hopping integrals as given by Eskes, Sawatzky, and Feiner.[28] This choice of parameters is motivated by the complete characterization of the multiplet structure by the Racah parameters in Ref. 28. The latter parameter set was supplemented by the crystal-field splitting between the $3d_{x^2-y^2}$ and $3d_{3z^2-1}$ states, as given by Grant and McMahan.[27] In order to facilitate comparisons with the experimental data, we have used the electronic notation in all the numerical results. The hopping parameters are:[27] $t_{pp}=0.65$ eV for the hopping between nearest $2p_\sigma$ or $2p_\pi$ orbitals, $t'_{pp}=0.35$ eV for the hopping between nearest $2p_\sigma$ and $2p_\pi$ orbitals, and $t_x=1.5$ eV, $t_z=0.5$ eV for the hybridization elements between $2p_\sigma$ and $3d_{x^2-y^2}$, $3d_{3z^2-1}$ orbitals, respectively. The CT energy between $2p_\sigma$ and $3d_{x^2-y^2}$ is $\Delta_\sigma=\varepsilon_x-\varepsilon_\sigma=3.5$ eV, while $\Delta_{xz}=\varepsilon_x-\varepsilon_z=0.6$ eV is the crystal-field splitting between $3d_{x^2-y^2}$ and $3d_{z^2}$ states. The value of the superexchange interaction $J$, has been found to be $J\sim 0.07-0.15$ eV by Raman scattering and neutron-scattering experiments.[40] In the present model we assume $J=0.15$ eV which is an accepted value in the literature.[28,37,41,42] The Coulomb energies calculated with the parameters of Ref. 28 are: $U(^3A_2)=5.3$, $U(^1E_1)=7.3$, and $U(^1A_2)=8.3$ eV. We note that the one-particle elements (hopping integrals and CT energy) are the same as in the sets determined from the local-density approximation (LDA) calculations,[26,27] while the Coulomb interactions are somewhat weaker. Thus, we overestimate here the strength of the Kondo coupling both by taking only the second-order expressions for the exchange interactions, and by accepting the lower limit for the $U$'s. Nevertheless, we are still in the range of applicability of the perturbation theory.

Before we address the results obtained for the spectral functions, let us analyze the behavior of the hole-magnon coupling in momentum space. As in the case of NiO,[23] this coupling vanishes at the $\Gamma$ point, increases both in the $\Gamma-M$ and in $\Gamma-X$ directions, and is at maximum at the $M$ point [see Eqs. (2.28)]. These symmetry-derived properties are also reproduced by the band structure as follows from the tight-binding model neglecting the hole-magnon couplings (see Fig. 1). The free oxygen bands are only slightly changed by $H_h^J$ corrections, with an additional splitting $\Delta E\simeq 0.3$ eV, increasing from $\Gamma$ towards the M point.

The full spectral functions $A_{\mu\mu}(\mathbf{k},\omega)$ ($\mu=1,2$) are presented in Fig. 2. Because the hole-magnon coupling vanishes, one finds at the $\Gamma$ point a (doubly degenerate) $\delta$-function-like peak. Going away from the $\Gamma$ point towards the $X$ point, the spectral functions become broader, while a bound state becomes visible at the threshold of the spectral functions, in both channels. This bound state carries, however, only little weight, while most of the spectrum is concentrated in the broad region at high energy, with the $z^2$ symmetry following more closely the one-particle dispersion of the oxygen states (see Fig. 1). In the latter case the Kondo interaction is much weaker and therefore the corrections to the one-particle picture are much less than in the $x^2-y^2$ channel. In the vicinity of the $M$ point the bound states become more visible in the $x^2-y^2$ channel. Interestingly, an antibound state at high energy is formed in the (11) direction in the $x^2-y^2$ channel simultaneously. Such a state has also been found in NiO for weaker Ni-O hybridizations than those assumed in Ref. 23.

The total density of states $A_\mu(\omega)$ of this two-band model

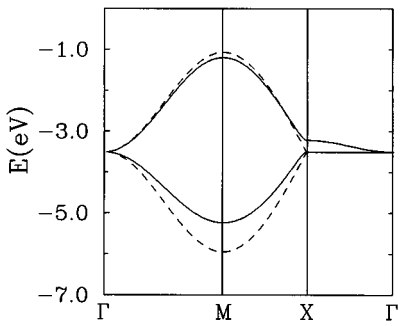


FIG. 1. The oxygen electron bands for $p_\sigma$ orbitals as obtained from the hole hopping terms given by Eqs. (2.11) and (2.12): $H_h^0$ (dashed lines) and $H_h^0+H_h^J$ (solid lines) for realistic parameters of $CuO_2$ planes (see Sec. III).

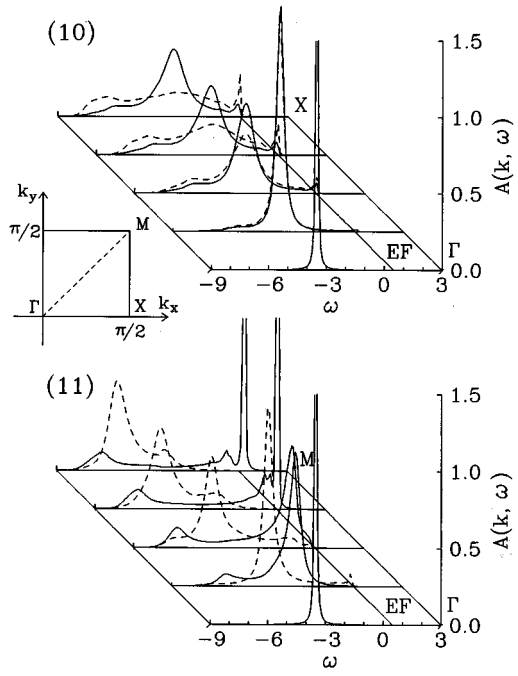


FIG. 2. Spectral functions, $A_{\mu\mu}(\mathbf{k},\omega)$ ($\mu=1,2$), including only $p_\sigma$ orbitals for $\mathbf{k}=(n\pi/8,0)$ in the (10) direction, and for $\mathbf{k}=(n\pi/8,n\pi/8)$ in the (11) direction ($n=0,1,2,3,4$), as obtained for the simplified $\sigma$ only model for an oxygen hole in the $CuO_2$ plane using the parameters of Refs. 27,28. Full and dashed lines correspond to the states of $d_{x^2-y^2}$ and $d_{z^2}$ symmetry, respectively. The inset shows the convention chosen for the BZ, with the Cu-O distance taken as the length unit $a=1$. Doping by $\sim 7\%$ holes results in the marked position of the Fermi level, $E_F$. The parameters as defined in Sec. III.

is shown in Fig. 3. Both the QP (at the threshold of the spectra) and the antibound states (with the maximum $\sim -6.5$ eV) come from the upper ($d_{x^2-y^2}$) oxygen band (see Fig. 3), while the $\pi$ states couple much weaker to magnons and plays thus a minor role in the formation of the propagating states. The total spectral weight of the propagating states at low energies does not exceed 10%. One can also distinguish a strong peak in both spectra (at $\sim -3.5$ eV)—this is

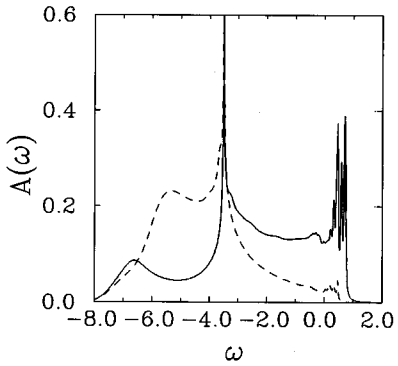


FIG. 3. The total density of electron states, $A_\mu(\omega)=(1/N)\Sigma\mathbf{k}A_{\mu\mu}(\mathbf{k},\omega)$ for $d_{x^2-y^2}$ (solid line) and $d_{z^2}$ (dashed line) symmetry states, respectively. The parameters as defined in Sec. III.

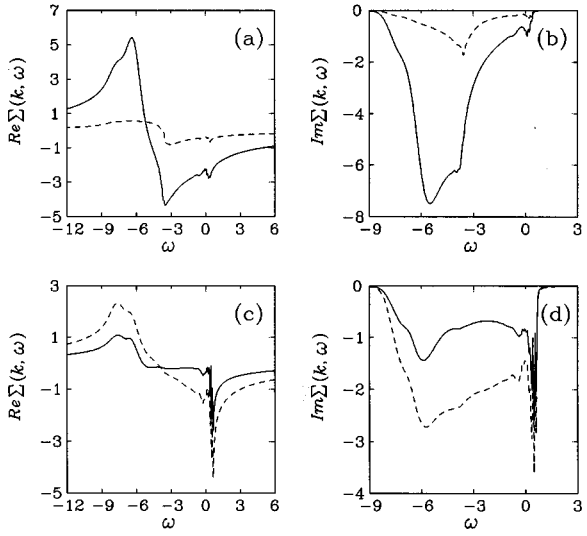


FIG. 4. Real and imaginary parts of the self-energy $\Sigma_{\mu\mu}(\mathbf{k},\omega)$ for the realistic parameters of $CuO_2$. Upper panels (a) and (b) correspond to the $M$ point, and lower ones (c) and (d) to the $X$ point in the BZ. Solid and dashed lines represent the two $e_g$ symmetries, respectively.

nothing else than the van Hove singularity of the independent electron bands which survive the hole-magnon scattering because this interaction vanishes at the $\Gamma$ point.

It is interesting to compare the behavior of $\Sigma_{\mu\mu}(\mathbf{k},\omega)$ for different points in the Brillouin zone (BZ). At the $M$ point (where the QP peak is the strongest) both the real and the imaginary parts of $\Sigma_{\mu\mu}(\mathbf{k},\omega)$ (2.30) are rather smooth functions of $\omega$ with only a small discontinuity at the QP state [Figs. 4(a) and 4(b)]. On the other hand, at the $X$ point (with the very weak QP peak) $\Sigma_{\mu\mu}(\mathbf{k},\omega)$ has many well visible oscillations in a narrow energy range [see Figs. 4(c) and 4(d)]. Such a big difference in the behavior of the self-energy is caused by the fact that the propagating states are build up near the $M$ point not far from the pure oxygen states (see the upper band on Fig. 1), whereas at the $X$ point the energy of the upper oxygen band is $\sim -3.5$ eV and the self-energy has to develop such strong oscillations in order to form the QP states at $\sim 4$ eV above the free states.

Let us turn back to the low-energy bound states. Their nature is similar to that found previously in NiO (Ref. 23)—they are similar to the Zhang-Rice local singlet states which can be derived in the limit of $J_K \gg t_{pp}$ and this will be further discussed towards the end of this section. They show a dispersion which is actually quite similar to the dispersion obtained with $t$-$t'$-$J$ models,[43] and to stress this point we show our results together with the dispersions with ARPES as measured in the highly doped, superconducting compound $Bi_2Sr_2CaCu_2O_{8+\delta}$ by Dessau *et al.*[9] in Fig. 5. These compare quite well, at least assuming that one can rigidly shift the bands under doping. This is of course nonsensical (the vacuum is of a completely different nature) and we will actually show in the next section that the scattering against the Néel order (neglected here) gives rise to substantial changes in the form of the dispersion. The real dispersions look more like the dispersion found in insulating samples, and the similarity suggested by Fig. 5 is just accidental.

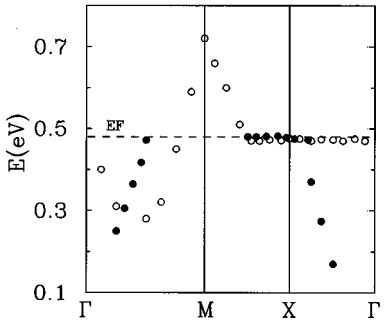


FIG. 5. The calculated ZR QP states in the spin-fermion model with oxygen $p_\sigma$ orbitals (empty circles) and the maxima measured in ARPES experiments by Dessau *et al.* (Ref. 9) (full circles). The Fermi energy (dashed line) is the same as in Fig. 2. Notice that this favorable comparison is merely accidental.

Let us now present the numerical results obtained in the more complete four-band spin-fermion model (2.25), as derived in Sec. II including also $3d_{xy}$ and $2p_\pi$ states in the basis set. The additional electronic structure parameters which had to be included are: $t_{xy}=0.7$ eV—hybridization between $2p_\pi$ and $3d_{xy}$ orbitals [obtained using the relation between the hopping elements for $b_1$ and $b_2$ symmetries: $t_{xy}=t_x/2$ (see Ref. 44)] and in agreement with Ref. 36; $\Delta_\pi=\varepsilon_{xy}-\varepsilon_\pi=1.3$ eV—the CT energy between $3d_{xy}$ and $2p_\pi$ orbitals; $U(^1T_1)=U(^1E_1)$ and $U(^3T_1)=U(^3A_2)$—the Coulomb repulsions for the new $d^8$ configurations ($^1T_1$ and $^3T_1$). In this case, the self-consistent calculations involve four oxygen bands which makes the numerical procedure more tedious. One expects that the QP states near the Fermi energy are still primarily determined by the holes of $\sigma$ character. In addition, it would be interesting to see whether similar QP structures are formed in the $\pi$ sector, as was the case in NiO.[23] The free oxygen bands in the four-band spin-fermion model (Fig. 6) are qualitatively similar to those found before using only $\sigma$ states (see Fig. 1). The features are the dispersions along the $\Gamma-X$ direction even when the second-order corrections to the bands are neglected, and the splitting at the $\Gamma$ point, which originates in the $t_{mn}^{\sigma\pi}$ hopping Eq. (2.11).

In the first instance, one can consider the $\sigma$ and $\pi$ sectors (see Figs. 7 and 8) as being independent. As expected, the spectral functions in the $\pi$ sector (Fig. 8) are basically those of the free holes, slightly changed (''shifted and broadened'') by the interactions with the magnons. Only along the $\Gamma-M$ direction there are more drastic changes due to the relatively strong hole-magnon vertex in this part of the BZ. Surprisingly, however, we find a rather large effect in the $\sigma$ sector (Fig. 7) coming from the presence of the $\pi$ states, despite the nominally small coupling between the two sectors. Although the $\sigma$ spectra look similar at high energies to the ones of the $\sigma$ only model, it is also seen that the pole strength of the low-energy QP states reduces drastically (Fig. 2): the QP states are barely recognizable along the $\Gamma-X$ directions in both $\sigma$ and $\pi$ symmetry sectors. This reduction of pole strength might as well be interpreted as a decrease of the binding energy of the Zhang-Rice-like states. The origin of this effect is easy to understand. From Eqs. (2.7) and (2.8) it follows that the Kondo couplings are *ferromagnetic* both in

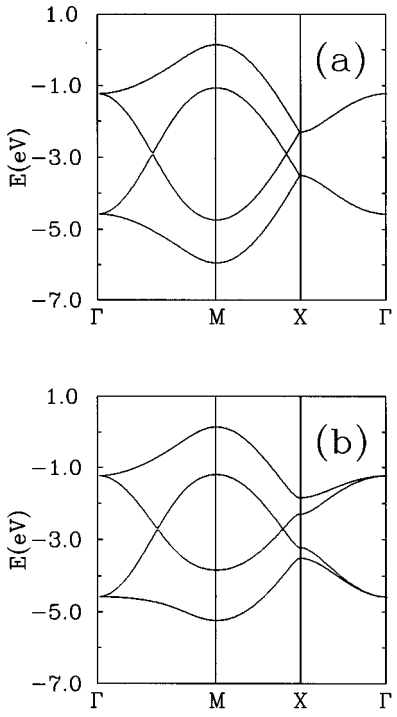


FIG. 6. Free oxygen electron bands in the spin-fermion model which includes $p_\sigma$ and $p_\pi$ oxygen orbitals without (a) and with (b) the three-site hopping terms given by $H_h^J$ The parameters as in Sec. III.

the $\pi$ sector, as in the $3z^2-1$ channel, while only in the $x^2-y^2$ channel the Kondo coupling is antiferromagnetic. The reason is that in the former two channels the Kondo exchange comes from virtual fluctuations into $d^8$ states involving two different orbitals ($x^2-y^2$, and $xy$ and $3z^2-1$ in the $\pi$ and $3z^2-1$ channels, respectively). The high spin (triplet) $d^8$ states of this kind lie at a lower energy than the singlet states because of Hund's rule, and this ferromagnetic sign is ''transferred'' to the low-energy sector. In the $x^2-y^2$ channel, on the other hand, only one orbital is available and the Kondo exchange carries therefore the usual ''kinetic'' antiferromagnetic sign. The latter is more strongly coupled and tends to produce the singletlike bound QP states. However, in the other channels there is also a tendency to form hole-spin bound states, which are however *triplet* (high spin) like. Because the free states in the $3z^2-1$ channel are at high energy, there is little left at low energies in this channel. This is different in the $\pi$ channel. The free dispersion of the lower lying free $\pi$ band follows the $x^2-y^2$-like band closely (Fig. 6), and the renormalized $\pi$ states already show up at quite low energies. *These low-energy, ferromagnetically correlated $\pi$ states act like ''pair-breakers'' on the singletlike, spin-hole bound states in the $x^2-y^2$ channel.* The surprise is in the numbers. The coupling between the $\pi$ and $\sigma$ channel is quite weak, but this small coupling is nevertheless able to change the outcomes quite substantially. We notice that we also found these ''high spin'' and ''low spin'' bound states in the context of NiO.[23] The main difference with the present case is that $J_K/t_{pp}$ is substantially larger in NiO than in cuprates, with the effect that both in the low spin and in the high spin channel the bound states are well developed.

TABLE I. Quasiparticle weight ($n=0$) and the norm $N^{(n)}_{\mathbf{k},1}$ ($n=1,2,3$) [given by Eq. (2.34)] at $\mathbf{k}=(\pi/2,\pi/2)$ ($M$ point) and at $\mathbf{k}=(\pi/2,0)$ ($X$ point) as a function of $J$ (in eV), found for the four-band model with normalization $N^{(3)}_{\mathbf{k},1}=1$ at $J=0.25$ eV.

| | $J$ | $n=0$ | $n=1$ | $n=2$ | $n=3$ |
|---|---|---|---|---|---|
| $\mathbf{k}=(\pi/2,\pi/2)$ | 0.025 | 0.3951 | 0.5845 | 0.5955 | 0.5968 |
| | 0.05 | 0.5132 | 0.7470 | 0.7565 | 0.7574 |
| | 0.10 | 0.6160 | 0.8753 | 0.8816 | 0.8821 |
| | 0.15 | 0.6697 | 0.9368 | 0.9414 | 0.9417 |
| | 0.20 | 0.7046 | 0.9729 | 0.9764 | 0.9766 |
| | 0.25 | 0.7310 | 0.9970 | 0.9998 | 1.0000 |
| $\mathbf{k}=(\pi/2,0)$ | 0.025 | 0.0076 | 0.0204 | 0.0217 | 0.0221 |
| | 0.05 | 0.0093 | 0.0244 | 0.0256 | 0.0260 |
| | 0.10 | 0.0119 | 0.0312 | 0.0325 | 0.0328 |
| | 0.15 | 0.0148 | 0.0400 | 0.0414 | 0.0417 |
| | 0.20 | 0.0174 | 0.0463 | 0.0478 | 0.0480 |
| | 0.25 | 0.0208 | 0.0556 | 0.0573 | 0.0575 |

Let us now address the precise nature of the low-energy, bound QP states. For this purpose, it is revealing to consider the nature of the ground-state wave function at different momenta, using Eq. (2.34). Let us first discuss the general nature of the problem. It is characterized by two parameters, $J_K/W$ and $J/W$ ($W$ is the bandwidth), which can be well compared in this large $S$ context with the electron-phonon coupling constant and the Debye frequency of the analogous lattice polaron problem. The small-polaron limit of the lattice problem is in fact analogous to the Zhang-Rice construction: the Zhang-Rice singlet can be looked at as a bound state of a hole and a local, large amplitude spin wave which is realized in the large $J_K/W$ limit. In this limit, the bound object has lost all its free kinetic energy and can only propagate through the lattice assisted by the exchange of the collective excitation. In the spin case, the latter part is described by the $t$-$J$ model which appears as ''infinitely strongly coupled'' in large $S$ (no free kinetic energy). Although at the end propagating states are found, these are dressed up with large numbers of magnons, using an analysis equivalent to Eq. (2.34).[33,43] This Zhang-Rice singlet/$t$-$J$ picture is however only accurate in the large $J_K/W$ limit. If $J_K/W<1$, this strong-coupling picture breaks down and one better thinks in terms of the free states which get shifted and broadened due to the hole-magnon scattering, as one sees happening in the $\pi$ and $3z^2-1$ channels in large parts of momentum space. In this limit, only a fraction of a magnon is attached to the hole.

In the $x^2-y^2$ channel, the problem is obviously well inside the intermediate coupling regime: $J_K$ and the free bandwidth $\sim t_{pp}$ are of the same order. The norms $N_{\mathbf{k},i}$ are a sensitive measure for the number of magnons involved in the formation of the bound state,[33,43] and these are summarized in Table I for $n=1,2,3$ magnons along the high-symmetry directions in the zone for different values of $J$. On the one hand, we find that $N_{\mathbf{k},i}$ increases with increasing superexchange $J$ in a similar way as in the $t$-$J$ model.[33,43] On the other hand, however, for a realistic value of $J=0.15$ eV, $N_{\mathbf{k},i}$ converges rapidly, much more rapidly than is the case in the $t-J$ model, taking ''realistic'' values for $t$ and $J$. At $J=0.15$ eV, the one magnon contribution is still substantial but the two and three magnon contributions have already become insignificant: $\sim 3\%$ ($\sim 0.5\%$), and $\sim 0.5\%$ ($\sim 0.03\%$) for $n=2$ and 3 at the $X$ ($M$) point, respectively (see Table I).

These results should be taken as a warning against too literal interpretations of the results derived from the $t$-$J$ model. As long as bound states are formed, it makes sense to use the $t$-$J$ model for *qualitative* purposes. However, it seems *impossible* to arrive at any quantitative conclusion regarding dispersions, etc., starting from the strong-coupling limit. Of course, one can augment the standard $t$-$J$ model with other corrections (such as ''on sublattice hopping'' $t'$), but since the real (spin-fermion) model is deep in the intermediate-coupling regime the number of these corrections is bound to proliferate. We notice that all existing approaches, mapping the full problem onto $t$-$J$ like models,[45,46] are in a deep sense uncontrollable because they are not able to recover the weak-coupling ($J_K/W<1$) limit.

## IV. ANTIFERROMAGNETIC SPLITTING IN THE OXYGEN BANDS

In this section we include the AF splitting of the oxygen bands due to the scattering against the Néel order parameter, which was neglected in the numerical analysis presented in Sec. III. Neglecting these splittings is actually quite unreasonable since they amount to the zeroth order in the large $S$ expansion. The only reason to do so was to keep the calculation including the $\pi$ bands tractable. In this section we will neglect the $\pi$ bands and focus on the $\sigma$ sector instead. One should keep in mind that the $\pi$ bands might give rise to corrections which are not unimportant in quantitative respects.

The two-band spin-fermion model [see Eq. (2.4)] including the scattering against the Néel order takes the following form in the $S\rightarrow\infty$ limit:

$$\widetilde{H}=H_{\mathrm{TB}}+H_h^{\mathrm{AF}}, \tag{4.1}$$

where $H_{\mathrm{TB}}$ is the $\sigma$-only model we considered in Sec. III, and

$$H_h^{\mathrm{AF}}=S\sum_{ijj'\sigma}\sum_{\xi\xi'=1,2}\lambda_\sigma J_{\xi\xi'}[a^\dagger_{j\xi\sigma}a_{j'\xi'\sigma}+\mathrm{H.c.}], \tag{4.2}$$

where $\lambda_\sigma=\pm$ for $\sigma=\uparrow,\downarrow$, respectively. The new elements lift the spin degeneracy of the oxygen bands. $H_h^{\mathrm{AF}}$ gives the usual coupling between the $\mathbf{k}$ and $\mathbf{k}+\mathbf{Q}$ states in the reciprocal space

$$H_h^{\mathrm{AF}}=\sum_{\mathbf{k}}\sum_{\xi\xi'}\alpha_{\xi\xi'}(\mathbf{k})[a^\dagger_{\mathbf{k}+\mathbf{Q},\xi\uparrow}a_{\mathbf{k},\xi'\uparrow}-a^\dagger_{\mathbf{k}+\mathbf{Q},\xi\downarrow}a_{\mathbf{k},\xi'\downarrow}], \tag{4.3}$$

where $\mathbf{Q}=(\pi/2,\pi/2)$ is the 2D nesting vector, $S=\frac{1}{2}$, and

$$\begin{aligned}
\alpha_{11}(\mathbf{k})&=-(J_{k,x^2-y^2}+J_{k,z^2})\sin(2k_x),\\
\alpha_{22}(\mathbf{k})&=-(J_{k,x^2-y^2}+J_{k,z^2})\sin(2k_y),\\
\alpha_{12}(\mathbf{k})&=2(J_{k,x^2-y^2}-J_{k,z^2})\cos k_x\sin k_y,\\
\alpha_{21}(\mathbf{k})&=2(J_{k,x^2-y^2}-J_{k,z^2})\cos k_y\sin k_x.
\end{aligned} \tag{4.4}$$

The oxygen subbands are now found from the diagonalization of the free hole Hamiltonian, $H_h^0+H_h^J+H_h^{\mathrm{AF}}$ which leads to the following $4\times4$ matrix problem, with the usual mixing between the $\mathbf{k}$ and $\mathbf{k}+\mathbf{Q}$ states for a given spin $\sigma$,

$$\begin{bmatrix} ([H_h^0]+[H_h^J])(\mathbf{k}) & \sigma[\alpha(\mathbf{k})] \\ \sigma[\alpha(\mathbf{k})] & ([H_h^0]+[H_h^J])(\mathbf{k}+\mathbf{Q}) \end{bmatrix}. \tag{4.5}$$

Using the initial unfolded BZ and expanding up to Gaussian order (as in Sec. III),

$$\widetilde{H}_{\mathrm{LSW}}=\sum_{\mathbf{k}\mu\sigma} E_\mu(\mathbf{k}) a^\dagger_{\mathbf{k},\mu\sigma} a_{\mathbf{k},\mu\sigma}+\sum_{\mathbf{q}} \omega_{\mathbf{q}} \beta^\dagger_{\mathbf{q}}\beta_{\mathbf{q}} + \frac{1}{\sqrt{N}} \sum_{\mathbf{kq},\mu\sigma} \widetilde{M}_{\mu\nu}(\mathbf{k},\mathbf{q}) a^\dagger_{\mathbf{k}-\mathbf{q},\sigma} a_{\mathbf{k},-\sigma}(\beta^\dagger_{\mathbf{q}}+\beta_{-\mathbf{q}}), \tag{4.6}$$

where $E_\mu(\mathbf{k})$ ($\mu=1,2$) are the eigenvalues of (4.5) in the unfolded BZ (see Fig. 9). The new vertex $\widetilde{M}_{\mu\nu}(\mathbf{k},\mathbf{q})$ has a form, which is different in different regions of the BZ (case $A-D$),

$$\widetilde{M}^2_{\mu\nu}(\mathbf{k},\mathbf{q})=\begin{cases} [A_{\mu\nu}(\mathbf{k},0,\mathbf{q},0,0,0)+A_{\mu\nu}(\mathbf{k},\mathbf{Q},\mathbf{q},0,2,2)]^2 & \\ +[A_{\mu\nu}(\mathbf{k},\mathbf{Q},\mathbf{q},\mathbf{Q},0,2)+A_{\mu\nu}(\mathbf{k},0,\mathbf{q},-\mathbf{Q},2,0)]^2 & \text{in case A,} \\ [A_{\mu\nu}(\mathbf{k},-\mathbf{Q},\mathbf{q},0,2,2)+A_{\mu\nu}(\mathbf{k},0,\mathbf{q},0,0,0)]^2 & \\ +[A_{\mu\nu}(\mathbf{k},0,\mathbf{q},Q,2,0)+A_{\mu\nu}(\mathbf{k},-\mathbf{Q},\mathbf{q},-\mathbf{Q},0,2)]^2 & \text{in case B,} \\ [A_{\mu\nu}(\mathbf{k},-\mathbf{Q},\mathbf{q},-\mathbf{Q},0,2)+A_{\mu\nu}(\mathbf{k},0,\mathbf{q},-\mathbf{Q},2,0)]^2 & \\ +[A_{\mu\nu}(\mathbf{k},0,\mathbf{q},0,0,0)+A_{\mu\nu}(\mathbf{k},-\mathbf{Q},\mathbf{q},-2\mathbf{Q},2,2)]^2 & \text{in case C,} \\ [A_{\mu\nu}(\mathbf{k},0,\mathbf{q},\mathbf{Q},2,0)+A_{\mu\nu}(\mathbf{k},\mathbf{Q},\mathbf{q},\mathbf{Q},0,2)]^2 & \text{in case D,} \\ +[A_{\mu\nu}(\mathbf{k},\mathbf{Q},\mathbf{q},2\mathbf{Q},2,2)+A_{\mu\nu}(\mathbf{k},0,\mathbf{q},0,0,0)]^2 & \end{cases} \tag{4.7}$$

with case (A): $|k_x+k_y|<\pi/2, |(k-q)_x+(k-q)_y|<\pi/2$; case (B): $|k_x+k_y|>\pi/2$, $|(k-q)_x+(k-q)_y|>\pi/2$; case (C): $|k_x+k_y|>\pi/2$, $|(k-q)_x+(k-q)_y|<\pi/2$, and case (D): $|k_x+k_y|<\pi/2$, $|(k-q)_x+(k-q)_y|>\pi/2$. We have introduced in Eq. (4.7) the following function to describe hole-magnon coupling:

$$A_{\mu\nu}(\mathbf{k},\mathbf{k}',\mathbf{q},\mathbf{q}',i,j)=(u_{\mathbf{q}+\mathbf{q}'}+v_{\mathbf{q}+\mathbf{q}'})\sum_{\xi\xi'} F_{\xi\xi'}(\mathbf{k}+\mathbf{k}',\mathbf{q}+\mathbf{q}') \times V^\mu_{\xi+i,\mathbf{k}-\mathbf{q}} V^\nu_{\xi'+j,\mathbf{k}}. \tag{4.8}$$

We emphasize that the leading contribution to the $\widetilde{M}^2_{\mu\nu}(\mathbf{k},\mathbf{q})$ comes from the $A_{\mu\nu}(\mathbf{k},0,\mathbf{q},0,0,0)$ elements, while the remaining terms in Eq. (4.7) are the AF corrections. The SCBA equations are the same as before, but one has to replace $\varepsilon_\mu(\mathbf{k})$ by $E_\mu(\mathbf{k})$ in the Green function [given by Eq. (2.29)], and $M_{\mu\nu}(\mathbf{k},\mathbf{q})$ by $\widetilde{M}_{\mu\nu}(\mathbf{k},\mathbf{q})$ in the self-energy [Eq. (2.30)].

The scattering against the Néel order affects strongly the oxygen bands. To keep the overall bandwidth the same, we have decreased the main $p-d$ hopping element from $t_x=1.5$ eV (Ref. 27) to $t_x=1.3$ eV, and adopted the standard Slater-Koster relation for the value of $t_z=t_x/\sqrt{3}$ (see Ref. 28). The remaining parameters are the same as in Sec. III. Comparing the free bands including the scattering against the Néel order (4.1) with those determined previously (see Figs. 1), one finds a large splitting of 3.8 eV at the $X$ point and along the edge of the AF (folded) BZ, as presented in Fig. 9. As a result, the upper band for $|k_x+k_y|>\pi/2$ is less dispersive than in the previous case (Fig. 1), and is well seperated from the rest of the band structure. Already on the level of the free bands we anticipate and enhancement of the binding energy of the hole-magnon bound states.

The symmetry of the hole-magnon vertex is the same as discussed in Sec. III, and infers that the hole decouples from the spin system at the $\Gamma$ point, because $\widetilde{M}_{\mu\nu}(\mathbf{k},\mathbf{q})\to0$ for $\mathbf{k}\to\Gamma$. The narrowness of the upper oxygen band in the AF structure leads to very strong QP states in this region [see Figs. 10 and 11 for $\mathbf{k}=(n\pi/8,n\pi/8)$ with $n=3,4$] which are in the present case more strongly bound and the threshold of the spectrum moves from $\sim0.5$ to $\sim1.0$ eV (compare Figs. 2 and 10). Another effect of the AF splitting is a considerable change in the shape of the incoherent part of the spectrum. Along the $\Gamma-X$ direction, the spectral weight is concentrated around the free oxygen bands with maxima at $\sim-3.5$ eV. Moreover, along the $\Gamma-M$ direction the incoherent states move towards lower energies [see Fig. 10 for $\mathbf{k}=(n\pi/8,n\pi/8)$ with $n=1,2$], and as a result one can see a very strong antibound state at the $M$ point (dashed line), whereas for the upper oxygen band the antibonding states, being so well pronounced at $\sim-6$ eV in the simplified model (Fig. 2), have disappeared in the present situation.

The AF splitting of the free hole states is also reflected in the density of states for both bands, represented by solid and dashed lines in Fig. 12. The QP part of the spectrum (at the threshold of the density of states in Fig. 12), together with low-energy incoherent part which results from the additional structures accompanying the QP peaks in Fig. 10 in the energy range from $\sim-1$ to $\sim1$ eV, is well seperated now (compare Figs. 3 and 12) from the completely incoherent part of the spectra, starting at energies below $\sim-1$ eV. Moreover, the formation of a narrow antibound state (near the $M$ point) is also visible in $A_{\mu\mu}(\omega)$ for $\omega\simeq-5$ eV (dashed line in Fig. 12).

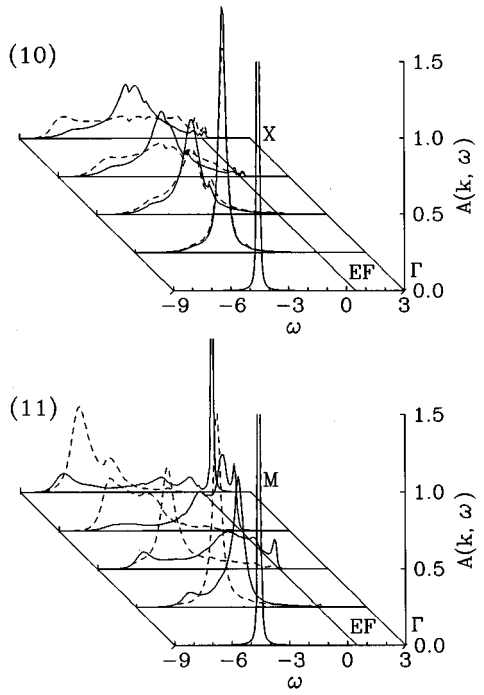


FIG. 7. Spectral functions of $e_g$ symmetry, $A_{\mu\mu}(\mathbf{k},\omega)$ ($\mu=1,2$), in the $\sigma-\pi$ model for $\mathbf{k}=(n\pi/8,0)$ in the (10) direction and for $\mathbf{k}=(n\pi/8,n\pi/8)$ in the (11) direction ($n=0,1,2,3,4$) for $CuO_2$ plane for $p_\sigma$ orbitals. Solid and dashed lines stand for the spectral functions of primarily $d_{x^2-y^2}$ and $d_{z^2}$ symmetry. Position of the Fermi level $E_F$ the same as in Figs. 2, 5; the parameters as in Sec. III.

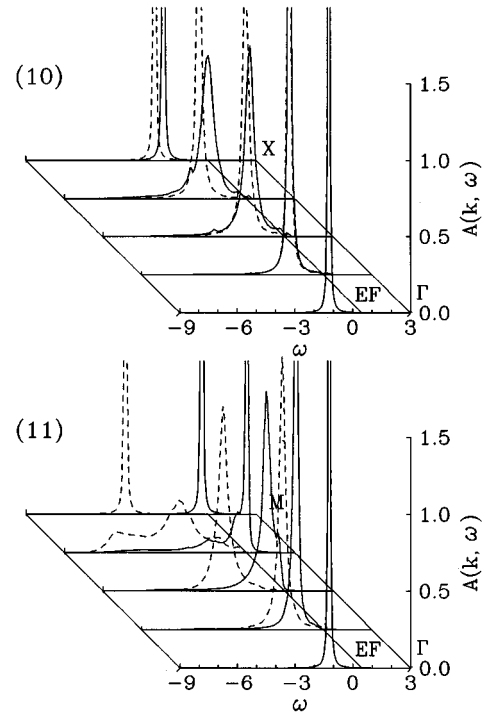


FIG. 8. Spectral functions, $A_{\mu\mu}(\mathbf{k},\omega)$ ($\mu=3,4$), in the $\sigma-\pi$ model for $\mathbf{k}=(n\pi/8,0)$ in the (10) direction and for $\mathbf{k}=(n\pi/8,n\pi/8)$ in the (11) direction ($n=0,1,2,3,4$) for the $\pi$-like states. Position of the Fermi level, $E_F$ and the parameters as in Fig. 7.

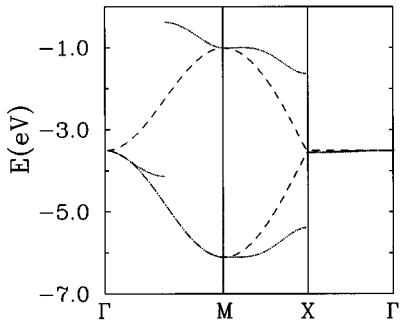


FIG. 9. The oxygen electron bands for $\sigma$ orbitals obtained from the Hamiltonian (2.11, 2.12) including the scattering against the static Néel background, as given by Eq. (4.3): $H_h^0+H_h^J$ (dashed lines) and $H_h^0+H_h^J+H_h^{\mathrm{AF}}$ (solid lines) for realistic parameters of $CuO_2$ planes.

The scattering against the Néel background changes the shape of the QP dispersions substantially, compared to the flawed result shown in Fig. 5. Comparing the present result shown in Fig. 11, with both the results for the dispersions in the heavily doped samples[9] and the experimental results as found from the *insulating* $Sr_2CuO_2Cl_2$, as presented by Wells *et al.*,[21] we find our calculated dispersion to be much closer to the latter case. Especially, we find the large flat piece in the $\Gamma-X$ direction to be well reproduced. Admittedly, the QP states have here rather low intensity, but could be identified, as shown in Fig. 13. We note, however, that the

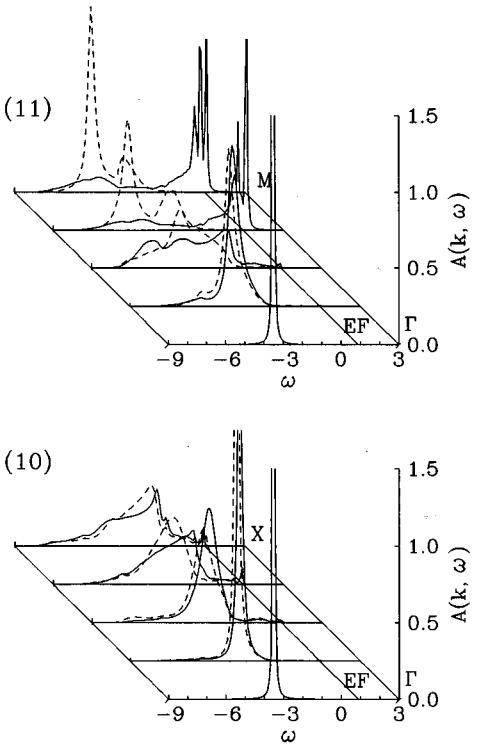


FIG. 10. Spectral functions, $A_{\mu\mu}(\mathbf{k},\omega)$ ($\mu=1,2$) for $\sigma$ orbitals, including the scattering of the oxygen holes against the static Néel background, for $\mathbf{k}=(n\pi/8,0)$ in the (10) direction and for $\mathbf{k}=(n\pi/8,n\pi/8)$ in the (11) direction ($n=0,1,2,3,4$) using the parameters as in Sec. IV and with the $E_F$ marked for 7% doping.

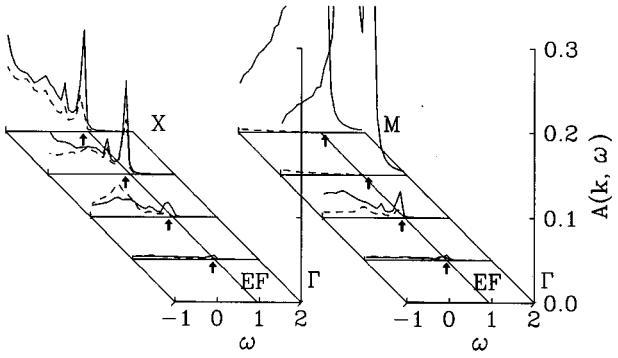


FIG. 11. QP states near the Fermi energy (indicated by arrows) in the spectral functions $A_{\mu\mu}(\mathbf{k},\omega)$ ($\mu=1,2$) for $\sigma$ orbitals, for $\mathbf{k}=(n\pi/8,0)$ in the (10) direction and for $\mathbf{k}=(n\pi/8,n\pi/8)$ in the (11) direction ($n=0,1,2,3,4$). The parameters and the value of $E_F$ are the same as in Fig. 10.

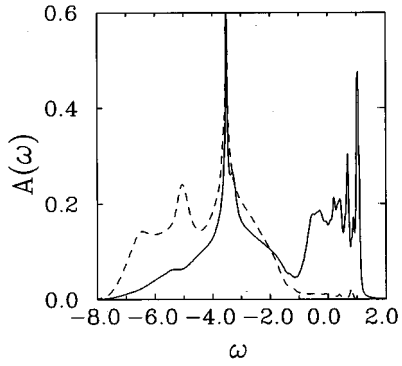


FIG. 12. The total density of electron states, $A_\mu(\omega)=(1/N)\Sigma\mathbf{k}A_{\mu\mu}(\mathbf{k},\omega)$ obtained from the model with the AF splitting in the oxygen bands. Solid and dashed lines stand for $d_{x^2-y^2}$ and $d_{z^2}$ spectral functions ($\mu=1,2$), respectively.

intensity would increase if the copper component would be calculated as well. The overall agreement is not perfect; especially, the calculation seems to indicate a rather flat maximum of the dispersion which lies a little way from the $M$ point in the $\Gamma-M$ direction. More importantly, we notice that our calculations reproduce rather accurately the *spectral weight* of the QP features seen in the experiments by Wells *et al.* as function of momentum:[21] the largest weights are found around the $M$ point, and the weights of the QP peaks rapidly diminish approaching the $\Gamma$ point (see Fig. 11). This reflects the disappearance of the hole-spin coupling at $\Gamma$.

## V. SUMMARY

We have presented an exhaustive study of the single-hole spectral function in the oxygen band region of insulating cuprates. Compared to existing studies mainly based on the $t-J$ model, our treatment has been more involved because we started with the spin-fermion model. This allowed us to address also the electronic states at higher energies, and in addition we were able to address in an unbiased way the effects of these higher lying states on the low-energy quasiparticle sector. In contrast to the $t$-$J$ model, the oxygen hole can move either by free and effective hopping processes between the neighboring oxygen orbitals, or via its coupling to the spin excitations (magnons) in the AF background of Cu spins. The numerical analysis performed within the SCBA demonstrates that the latter processes dominate always at the low-energy scale and lead to the formation of QP states with low dispersion. As in the $t$-$J$ model,[11] the dispersion is determined by the exchange interaction $J$, and one may wonder whether the oxygen hopping processes make similar modification of the dispersion in the present case, as the effective next-neighbor hopping in the $t$-$J$ model.[43]

Furthermore, using both the second-order expansion and the limited basis set of orbitals we have amplified the tendency towards the Zhang-Rice (ZR) localization. But we find it very encouraging that these states have survived at almost unchanged positions within the extended four-band spin-fermion model for $CuO_2$ plane. Of course, the QP states (disturbed by holes in $t_{2g}$ configurations which mix with the $e_g$ sector via $t'_{pp}$ hoppings) are less visible than the ZR singlet with pure $e_g$ symmetry, but the present approach is in any case not sufficient to reproduce the intensities of the QP peaks. Therefore, we claim that the two-band model is representative and gives already a realistic description of the electronic states in HTSO's. We find it also very encouraging that our QP band agrees quite well with the dispersion of the singlet pole found in the sophisticated perturbative treatment of the three-band model by Unger and Fulde[22] which captures essentially the same corrections to the bound state dispersion as the present spin-fermion model. On the contrary, in the mean-field slave-boson approach one has to assume an unrealistically large CT energy in order to reproduce a narrow band near $E_F$.[22]

Our main conclusions are:

(i) We find reasons to criticize the use of $t$-$J$ models to consider *quantitative* aspects of the quasiparticle properties. Especially, favorable comparisons like the one in our Fig. 5 but based on the $t$-$J$ model, should be regarded as mere accidents. Our main criticism is straightforward and undeniable: in terms of the bare (spin-fermion) the problem is in the middle of the intermediate-coupling regime, and starting from the strong-coupling (Zhang-Rice, $t$-$J$) side one is bound to fail in quantitative regards, because of the proliferation of correction terms. This is best illustrated with our main result of Fig. 13, which does not look like any dispersion derived from a $t$-$J$-type model. In addition, we found a surprisingly large effect on the ''singlet'' quasiparticle sector coming from the admixing of the higher lying $\pi$ states. As we explained, this can be rationalized in terms of the ferromagneticlike correlations, characteristic for the low-lying $\pi$ states, which should be quite effective in disturbing the singletlike coherence in the $\sigma$-like QP sector. Unfortunately, we did not manage to include the effects of the $\pi$ bands in a fully realistic manner, and here remains room for further improvements.

(ii) Our calculations force us to conclude that bandlike features should exist at higher energies in the oxygen band region. In fact, we do not find any reason for the cuprates to be different in this regard than NiO, where these ''oxygen band'' features are quite clearly seen experimentally.[47] Furthermore, oxygen band features should have a better chance

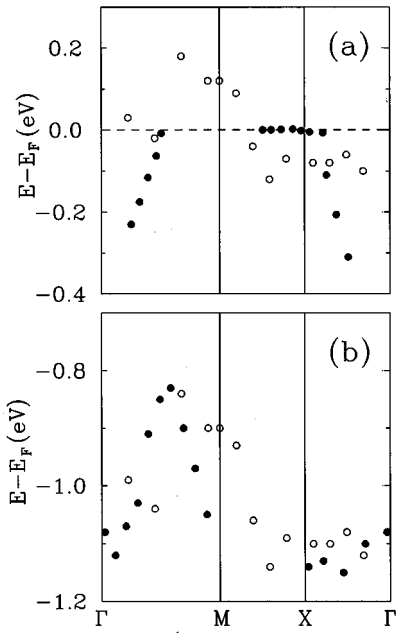


FIG. 13. Comparison between the QP dispersion, calculated from the $\sigma$ only model including the scattering against the Néel background and the experimental data: (a) calculated QP dispersion (empty circles) and the maxima measured in ARPES experiments by Dessau *et al.* in a highly doped cuprate (Ref. 9) (solid circles); (b) The same dispersion, but now compared with the ARPES experiments by Wells (Ref. 21) (solid circles) in an insulating compound (Ref. 49). One sees that the calculated dispersion is in fact much closer to the measured dispersion in the insulator.

to survive in the cuprates than in NiO because (a) the hole-magnon couplings are less strong in the cuprates, and (b) the two-dimensional nature of the cuprates simplifies the experiments. In the first instance, our prediction of strong momentum dependences in the oxygen band region (Figs. 7, 8, and 10) are based on symmetry: the hole-magnon vertex is strongly momentum dependent. At the $\Gamma$ point the bands become free, and in the neighborhood of the $\Gamma$ point the hole-magnon scattering is rather weak, translating in slightly ''shifted and broadened'' band states. Only in the $x^2-y^2$ channel the coupling grows rather large, while in the $\pi$ and $3z^2-1$ channels the coupling is weak enough that one would expect well defined, lifetime broadened band states of this character to persist in large parts of the BZ. No dispersing features have been seen in the oxygen band region by ARPES. We believe that this relates to a mere experimental problem: the broad humps seen in experiment are likely superpositions of the different band states, obscuring the dispersive nature of the individual bands. We hope that our work will be helpful in guiding future experiments aimed at disentangling the various contributions to the one-hole spectral function.

Altogether, we believe that a closer inspection of the realistic 2D spin-fermion models will resolve several still open questions on the QP nature of the low-energy peaks measured in the ARPES experiments in strongly correlated systems. As the present model deals only with $p$-type cuprates it would be of great interest to extend it to $n$-type HTSO with holes removed by doping from Cu orbitals within the $CuO_2$ planes. We also hope that a future extension to finite temperatures[48] could give valuable information about the thermodynamic properties of the strongly correlated systems.

## ACKNOWLEDGMENTS

J.B. and A.M.O. acknowledge the financial support by the Committee of Scientific Research (KBN) of Poland, Project No. 2 P03B 144 08. J.Z. ackowledges financial support by the Royal Dutch Academy of Sciences (KNAW).

*Permanent address: Institute of Physics, Jagellonian University, Reymonta 4, PL-30 059 Kraków, Poland.

[1] J. G. Bednorz and K. A. Müller, Z. Phys. B **64**, 189 (1986).
[2] For a review see, E. Dagotto, Rev. Mod. Phys. **66**, 763 (1994).
[3] J. Zaanen and G. A. Sawatzky, Prog. Theor. Phys., Suppl. **101**, 231 (1990).
[4] Y. Kitaoka *et al.*, Physica C **153-155**, 733 (1988); J. M. Tranquada *et al.*, Phys. Rev. B **38**, 2477 (1988).
[5] K. C. Haas, in *Solid State Physics: Advances in Research and Applications*, edited by H. Ehrenreich and D. Turnbull (Academic, Orlando, 1989), Vol. 42, p. 213.
[6] F. C. Zhang and T. M. Rice, Phys. Rev. B **37**, 3759 (1988).
[7] J. Zaanen and A. M. Oleś, Phys. Rev. B **37**, 9423 (1988).
[8] P. W. Anderson, G. Baskaran, Z. Zou, and T. Hsu, Phys. Rev. Lett. **58**, 2790 (1987).
[9] D. S. Dessau *et al.*, Phys. Rev. Lett. **71**, 2781 (1993).
[10] Z. X. Shen and D. S. Dessau, Phys. Rep. **253**, 1 (1995).
[11] K. J. von Szczepanski, P. Horsch, W. Stephan, and M. Ziegler, Phys. Rev. B **41**, 2017 (1990).
[12] G. Martínez and P. Horsch, Phys. Rev. B **44**, 317 (1991).
[13] F. Marsiglio, A. E. Ruckenstein, S. Schmitt-Rink, and C. M. Varma, Phys. Rev. B **43**, 10 882 (1991).
[14] S. Schmitt-Rink, C. M. Varma, and A. E. Ruckenstein, Phys. Rev. Lett. **60**, 2793 (1989).
[15] C. L. Kane, P. A. Lee, and N. Read, Phys. Rev. B **39**, 6880 (1989).
[16] P. Prelovšek, Phys. Lett. A **126**, 287 (1988).
[17] A. E. Ruckenstein, P. J. Hirschfeld, and J. Appel, Phys. Rev. B **36**, 857 (1987); A. M. Oleś, Int. J. Mod. Phys. **3**, 1789 (1989).
[18] E. Dagotto, R. Joynt, A. Moreo, S. Bacci, and E. Gagliano, Phys. Rev. B **41**, 9049 (1990); Z. Liu and E. Manousakis, *ibid.* **45**, 2425 (1992); D. Poilblanc, T. Ziman, H. J. Schulz, and E. Dagotto, *ibid.* **47**, 14 267 (1993).
[19] E. Dagotto, A. Nazarenko, and M. Boninsegni, Phys. Rev. Lett. **73**, 728 (1994).
[20] A. Nazarenko *et al.*, Phys. Rev. B **51**, 8676 (1995).
[21] B. O. Wells *et al.*, Phys. Rev. Lett. **74**, 964 (1995).
[22] P. Unger and P. Fulde, Phys. Rev. B **47**, 8947 (1993).
[23] J. Bała, A. M. Oleś, and J. Zaanen, Phys. Rev. Lett. **72**, 2600 (1994).
[24] C. M. Varma, S. Schmitt-Rink, and E. Abrahams, Solid State Commun. **62**, 681 (1987); V. J. Emery, Phys. Rev. Lett. **58**, 2794 (1987).
[25] A. M. Oleś, J. Zaanen, and P. Fulde, Physica B **148**, 260 (1987); J. Dutka and A. M. Oleś, Phys. Rev. B **43**, 5622 (1991).
[26] M. S. Hybertsen, M. Schlüter, and N. E. Christensen, Phys. Rev. B **39**, 9028 (1989); A. K. McMahan, J. F. Annett, and R. M. Martin, *ibid.* **42**, 6268 (1990).

[27] J. B. Grant and A. K. McMahan, Phys. Rev. B **46**, 8440 (1992).
[28] H. Eskes, G. A. Sawatzky, and L. F. Feiner, Physica C **160**, 424 (1989).
[29] C.-X. Chen, H.-B. Schüttler, and A. J. Fedro, Phys. Rev. B **41**, 2581 (1990); H.-B. Schüttler and A. J. Fedro, *ibid.* **45**, 7588 (1992).
[30] M. Meinders, H. Eskes, and G. A. Sawatzky, Phys. Rev. B **48**, 3916 (1993).
[31] J. Zaanen, A. M. Oleś, and P. Horsch, Phys. Rev. B **46**, 5798 (1992).
[32] G. F. Reiter, Phys. Rev. B **49**, 1536 (1994).
[33] A. Ramšak and P. Horsch, Phys. Rev. B **48**, 10 559 (1993).
[34] A. M. Oleś and J. Zaanen, in *Recent Progress in Many-Body Theories*, edited by I. Avishai (Plenum, New York, 1990), Vol. 2, p. 55; M. Grilli, C. Castellani, and C. Di Castro, Phys. Rev. B **42**, 6233 (1990); F. Bucci, C. Castellani, C. Di Castro, and M. Grilli, *ibid.* **52**, 6880 (1995).
[35] O. Gunnarsson *et al.*, Phys. Rev. B **41**, 4811 (1990); H. Eskes and G. A. Sawatzky, Phys. Rev. Lett. **61**, 1415 (1988).
[36] A. K. McMahan, R. M. Martin, and S. Satpathy, Phys. Rev. B **38**, 6650 (1988).
[37] J. F. Annett, R. M. Martin, A. K. McMahan, and S. Satpathy, Phys. Rev. B **40**, 2620 (1989).
[38] F. Mila, Phys. Rev. B **38**, 11 358 (1988); L. H. Tjeng, H. Eskes, and G. A. Sawatzky, in *Strong Correlations and Superconductivity*, edited by H. Fukuyama, S. Maekawa, and A. P. Malozemoff, Springer Series in Solid State Physics, Vol. 89 (Springer-Verlag, Berlin, 1989).
[39] E. B. Stechel and D. R. Jennison, Phys. Rev. B **38**, 4632 (1988); **38**, 8873 (1988).
[40] S. L. Cooper *et al.*, Phys. Rev. B **42**, 10 785 (1990); S. Sugai, S. Shamoto, and M. Sato, *ibid.* **38**, 6436 (1988); Y. Ohta, T. Tohyama, and S. Maekawa, Phys. Rev. Lett. **66**, 1228 (1991); G. Shirane *et al.*, *ibid.* **59**, 1613 (1987); Y. Endoh *et al.*, Phys. Rev. B **37**, 7443 (1988).
[41] H. Eskes and J. H. Jefferson, Phys. Rev. B **48**, 9788 (1993).
[42] T. Tohyama and S. Maekawa, Phys. Rev. B **49**, 3596 (1994).
[43] J. Bała, A.M. Oleś, and J. Zaanen, Phys. Rev. B. **52**, 4597 (1995).
[44] H. Eskes, L. H. Tjeng, and G. A. Sawatzky, Phys. Rev. B **41**, 288 (1990).
[45] M. S. Hybertsen, E. B. Stechel, M. Schlüter, and D. R. Jennison, Phys. Rev. B **41**, 11 068 (1990).
[46] L. F. Feiner, J. H. Jefferson, and R. Raimondi, Phys. Rev. B **53**, 8751 (1996); R. Raimondi, J. H. Jefferson, and L. F. Feiner, *ibid.* **53**, 8774 (1996).
[47] Z. X. Shen *et al.*, Phys. Rev. Lett. **64**, 2442 (1990); Phys. Rev. B **44**, 3604 (1991).
[48] N. M. Plakida, V. S. Oudovenko, and V. Yu. Yushankhai, Phys. Rev. B **50**, 6431 (1994).
[49] Our numerical results have been shifted down in energy in order to obtain the best fit to the experiment. Here we are comparing the results with insulating $Sr_2CuO_2Cl_2$ and the Fermi energy can be put at arbitrary position above the oxygen spectrum.